Bis-Azide Low-Band Gap Cross-Linkable Molecule N 3 -[CPDT(FBTTh 2) 2] to Fully Thermally Stabilize Organic Solar Cells Based on P3HT:PC 61 BM

Hussein Awada, Thérèse Gorisse, Romain Peresutti, Thomas Tjoutis, Joël Moreau, Guillaume Wantz, Olivier Dautel

ACS OMEGA

Article

http://pubs.acs.org/journal/acsodf

Bis-Azide Low-Band Gap Cross-Linkable Molecule N_3-[CPDT(FBTTh$_2$)$_2$] to Fully Thermally Stabilize Organic Solar Cells Based on P3HT:$PC_{61}BM$

Hussein Awada,[†,§] Thérèse Gorisse,[‡,§] Romain Peresutti,[†] Thomas Tjoutis,[†] Joel J. E. Moreau,[†] Guillaume Wantz,*[,‡] and Olivier J. Dautel*[,†]

[†]Institut Charles Gerhardt de Montpellier, Laboratoire AM2N, UMR CNRS 5253, ENSCM 8 rue de l'Ecole Normale, 34296 Montpellier, France

[‡]Université de Bordeaux, Institut Polytechnique de Bordeaux, Laboratoire IMS, UMR CNRS 5218, 16 Avenue Pey Berland, F-33607 Pessac, France

Supporting Information

ABSTRACT: We synthesized a novel bis-azide low-band gap cross-linkable molecule N_3-[CPDT(FBTTh$_2$)$_2$] with wide absorption. This compound is of interest as an additive in polymer/fullerene bulk heterojunction solar cells. In addition to providing efficient thermal stabilization of the morphology, the additive can harvest additional solar light compared with pristine poly(3-hexyl thiophene) to improve the power-conversion efficiency (PCE). The additional donor material was visualized from the appearance of additional external quantum efficiency contributions between 650 and 800 nm. An open-circuit voltage increase of ∼2% compensates the decrease in the short-circuit current of ∼2% to achieve a fully thermally stabilized PCE of 3.5% after 24 h of annealing at 150 °C.

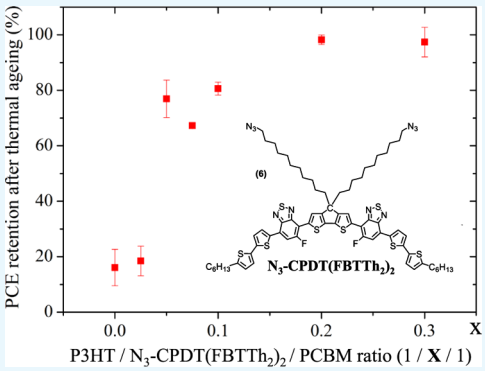

INTRODUCTION

Bulk heterojunction organic solar cells (BHJ-OSCs) have attracted a considerable amount of attention in recent years owing to their potential of providing efficient,[1] lightweight,[2] and low-cost manufacturing[3] through roll-to-roll coating and inkjet printing on flexible substrates. To be commercialized, ideal organic solar cells should present a constant performance of efficiency and durability, ascribed to a stable morphology. Breaking the 10% efficiency barrier in organic photovoltaic OSCs has been achieved for BHJ architectures based on conjugated polymers and small molecules with fullerene combinations after being a target over the last 2 decades.[1,4] Although, this efficiency still lags behind that of inorganic solar cells, it makes them very promising and potential candidates for future renewable energy needs. The key points that provide this significant enhancement are optimized design strategies, synthetic protocols, and device fabrication procedures.[5,6] Various fabrication techniques, such as solution processing by changing the spin-coated solvent[7] or incorporating a solvent additive[8] as well as postprocessing treatment: thermal annealing[9] or solvent annealing,[10] were essential to improve the solar cell efficiency. This was based on controlling the ordering of the π-conjugated materials in the solid state and nanophase segregation between the donor and acceptor materials within an exciton diffusion length scale of ∼10 nm.[11] However, the active layer (AL) is susceptible to degradation: a phase separation occurs between its components after aging.[12] The formation of micron-sized phenyl-C_{61}-butyric acid methyl ester ($PC_{61}BM$) crystals disrupts the ordering of the molecules and will negatively affect the charge diffusion, separation, and transport. This directly results in a huge drop in the power-conversion efficiency (PCE).[13] To address this limitation and suppress the crystallization of PCBM, cross-linkable groups incorporated on electron donor materials,[14−18] acceptors,[19−22] and small molecules[23,24] were reported, offering a locked and long-term thermally stable morphology. In parallel, two research groups recently turned their attention toward developing an innovative strategy to control the morphology and stability in one step. In this context, two dual functional additives were synthesized, with either a bifunctional azide cross-linker, such as 1,10-diazidodecane[25] and 1,6-diazidohexane (DAZH),[26] or a trifunctional azide cross-linker, such as tris(4-(5′-(3-azidopropyl)-2,2′-bithiophen-5-yl)phenyl)amine (TBT-N_3),[27] and incorporated into BHJ-OSCs. The dual functional behaviour of the additives resulted in the improvement of the photovoltaic performances and a retention of high PCE after prolonged thermal aging. On the basis of a similar concept, incorporating an additional donor material into binary BHJ-OSCs could broaden the absorption range and therefore increase the short-circuit current (J_{sc}). We

Received: December 7, 2016
Accepted: January 31, 2017
Published: April 7, 2017

DOI: 10.1021/acsomega.6b00476
ACS Omega 2017, 2, 1340−1349

Scheme 1. Synthetic Strategy for N_3-[CPDT($FBTTh_2$)$_2$] (6)

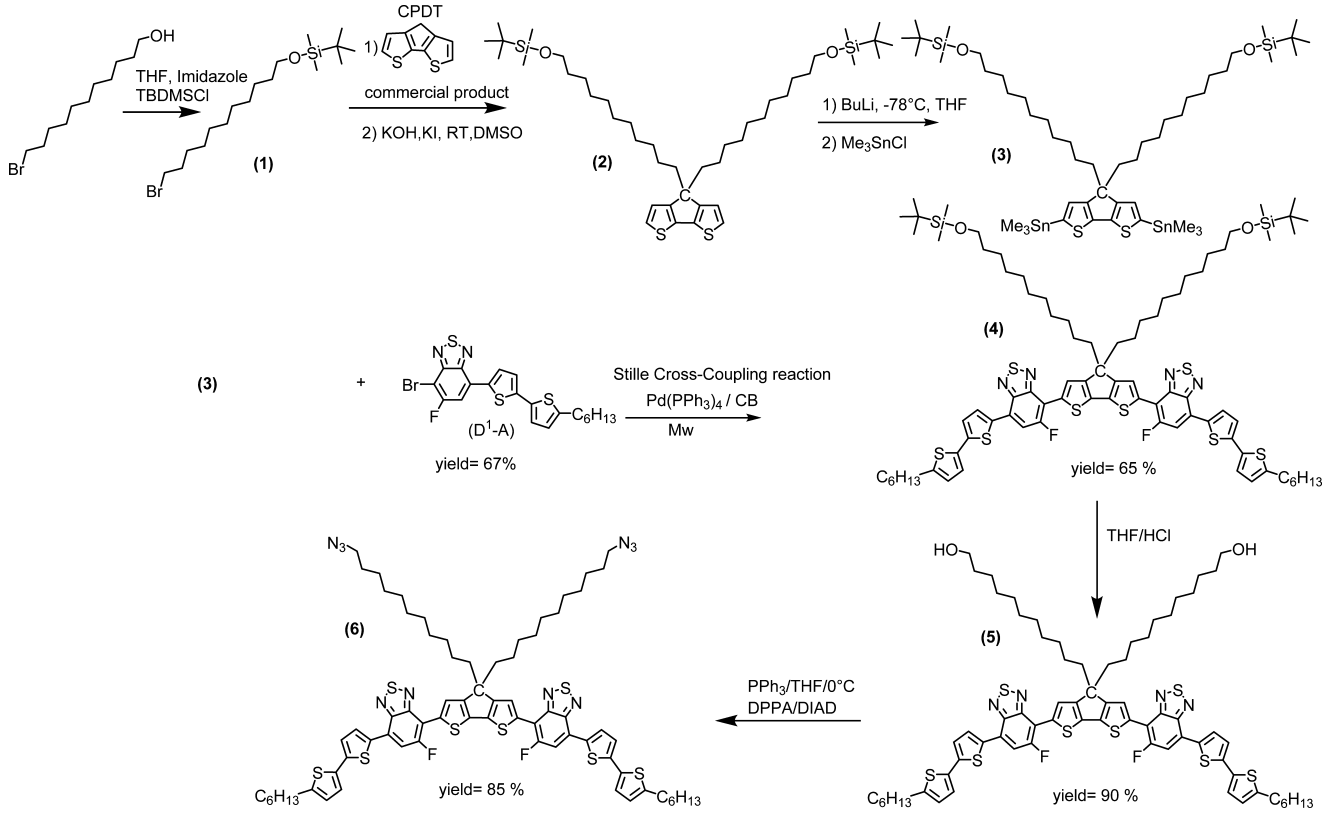

found that it is highly desirable to design new molecular architectures of dual function additives that can readily add to the spectral absorption besides their role in stabilization of the morphology. Therefore, an ideal solar cell device with enhanced efficiency and stability could be commercialized.

Herein, we present a description of the synthetic pathway utilized by us to insert a cross-linkable azide function into molecular donor 4-4′-bis(undecane)dicyclopenta[2,1-*b*:3,4-*b*′]-dithiophene-bis(5-fluoro-7-(5′-hexyl-[2,2′-bithiophene]-5-yl)-benzo[*c*][1,2,5]thiadiazole (CPDT($FBTTh_2$)$_2$, with a modular (D^1-A−D^2-A−D^1) architecture. Molecules with a similar structure have a good performance in organic solar cells, as previously reported.[28,29] The dual additive effect is demonstrated when the compounds are incorporated into the well-known poly(3-hexyl thiophene) (P3HT):$PC_{61}BM$ system.[24] Through primary optimization of the photovoltaic performance, the OPV cells show a PCE of 3.5%, which drops to 0.5% upon aging at 150 °C for 24 h. However, incorporation of an additive with a ratio of 0.2 wt/wt is sufficient to fully stabilize the efficiency after aging, where an additional external quantum efficiency (EQE) peak between 650 and 750 nm partially overcomes the loss of short-circuit current (J_{sc}) caused by the additive (50% of the drop is recovered by the additional EQE peak). Indeed, this new class of cross-linkable additives is promising for integration into organic solar cells, inducing thermally stable and highly efficient devices.

RESULTS AND DISCUSSION

Two synthetic pathways have been utilized in this study to substitute the 4,4′-position of CPDT with a linear alkyl chain bearing different functional groups (N_3, Br) to achieve a CPDT-based molecule in fewer steps[33] (Scheme S1 in the Supporting Information). Several attempts were made to stannylate such molecules, without any success. Despite selective lithiation at the *α*-position with *n*-BuLi, the reactivity of the functional groups leads to cyclization of the alkyl chain within the aromatic ring, and degradation of the molecules was observed. For the above-mentioned reasons, it was necessary to develop an alternative and efficient route for obtaining stable functionalized alkylated CPDT upon stannylation. A *tert*-butyldimethylsilyl ether (TBDMS)-protected undecyl bromine chain (**1**) was chosen to ensure stability of the alcohol functional group (OH), which can be converted into azide functionality upon designing the final molecule and the long alkyl chain (C_{11}) to increase the solubility. An overview of all synthetic steps for the synthesis of N_3-[CPDT($FBTTh_2$)$_2$] is presented in Scheme 1.

First, an efficient route was developed for obtaining TBDMS-functionalized CPDT (**2**) using KOH in dimethyl sulfoxide (DMSO) and a catalytic amount of KI. Then, selective lithiation at the *α*-position and stannylation with trimethyltin chloride provided molecule **3** in a high yield (99%). Thereafter, the D^1-A−D^2-A−D^1 structure of the [CPDT($FBTTh_2$)$_2$] molecule (**4**) was synthesized via a microwave-assisted Stille cross-coupling reaction using 4-bromo-5-fluoro-7-(5′-hexyl-[2,2′-bithiophene]-5-yl)benzo[*c*][1,2,5]thiadiazole (D^1-A), molecule **3**, and $Pd(PPh_3)_4$ as the catalytic system at an elevated temperature in chlorobenzene. Furthermore, deprotection of the TBDMS group of molecule **4** was performed in acidified tetrahydrofuran (THF) using HCl. After each step, [CPDT($FBTTh_2$)$_2$] molecules **4** and **5** were purified by washing with copious amounts of methanol and ethanol and then carrying out silica gel column chromatography. Finally, direct conversion of the alcohol to the azide was achieved via a one-step azidation reaction, according to a previously reported

DOI: 10.1021/acsomega.6b00476
ACS Omega 2017, 2, 1340−1349

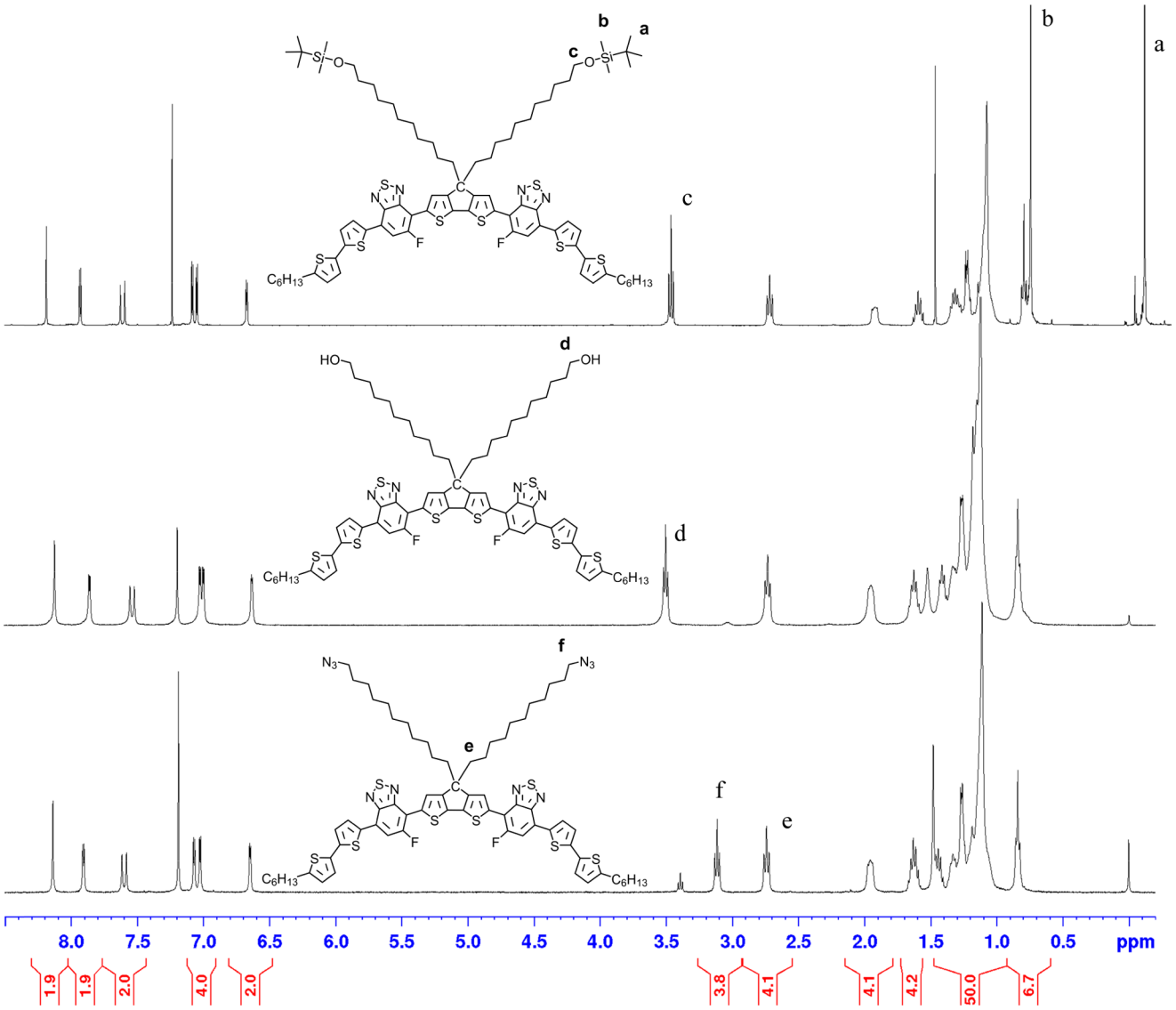

Figure 1. ^{1}H NMR spectra (400 MHz, $CDCl_3$) of TBDMS (**4**)-, OH (**5**)-, and N_3 (**6**)-functionalized [CPDT(FBTTh$_2$)$_2$].

procedure,[34,35] that used diphenylphosphoryl azide, di-*tert*-butylazidocarboxylate (DIAD), and triphenylphosphine (PPh_3) in anhydrous THF under an inert atmosphere. The azidated molecule was recovered after precipitation in methanol and found to contain 85% of azidated side chains.

The chemical structures of the [CPDT(FBTTh$_2$)$_2$] molecules were identified by ^{1}H NMR spectroscopy, ^{13}C NMR spectroscopy, matrix-assisted laser desorption ionization time-of-flight mass spectrometry (MALDI-TOFMS), and IR spectroscopy, and their purity was evaluated by high-performance liquid chromatography (HPLC). Figure 1 shows a superposition of the ^{1}H NMR spectra of TBDMS (**4**)-, OH (**5**)-, and N_3 (**6**)-functionalized [CPDT (FBTTh$_2$)$_2$]. In these spectra, the end groups were identified by their chemical shifts and splitting patterns. The spectrum of TBDMS−[CPDT-(FBTTh$_2$)$_2$] showed all of the characteristic signals of [CPDT(FBTTh$_2$)$_2$] and two additional signals (a and b) at 0.88 and 0.01 ppm (CH_3, s), corresponding to the methyl protons of the TBDMS-protected group. Total deprotection was confirmed from the OH−[CPDT(FBTTh$_2$)$_2$] spectrum, where the methyl proton signals of TBDMS completely disappeared and the signal corresponding to the methylene proton's (c) neighboring oxygen atom was shifted from 3.52 to 3.55 ppm. Finally, successful insertion of the azide functional group was confirmed by the shift in the methylene signal of the neighboring alcohol (d) from 3.55 to 3.17 ppm. Comparing the integration of protons, (e) 2.8 ppm, corresponding to four protons and (f) 3.17 ppm, corresponding to protons of methylene adjacent to the azide moiety, a maximum conversion of greater than 85% was calculated. The conversion value obtained is acceptable and similar to that in previously reported studies that used direct conversion of alcohol into azide.[34,35] Although the unreacted OH derivative (**5**) could not be eliminated after several attempts, confirmed by HPLC, this should not affect the performances because the OH residue in itself could be an interesting functionality that enhances the stability of organic solar cells when inserted into the CPDT alkyl chain.[36]

MALDI-TOF analysis and IR spectroscopy were used to confirm the successful insertion of azide functionality (Figures S8 and S10). First, the calculated exact masses of molecules **4**, **5**, and **6** were in agreement with the obtained MALDI mass spectra. The exact molar mass of N_3-[CPDT(FBTTh$_2$)$_2$] was clearly identified by the signal at 1368.5 g mol^{-1}. In addition, a

DOI: 10.1021/acsomega.6b00476
ACS Omega 2017, 2, 1340−1349

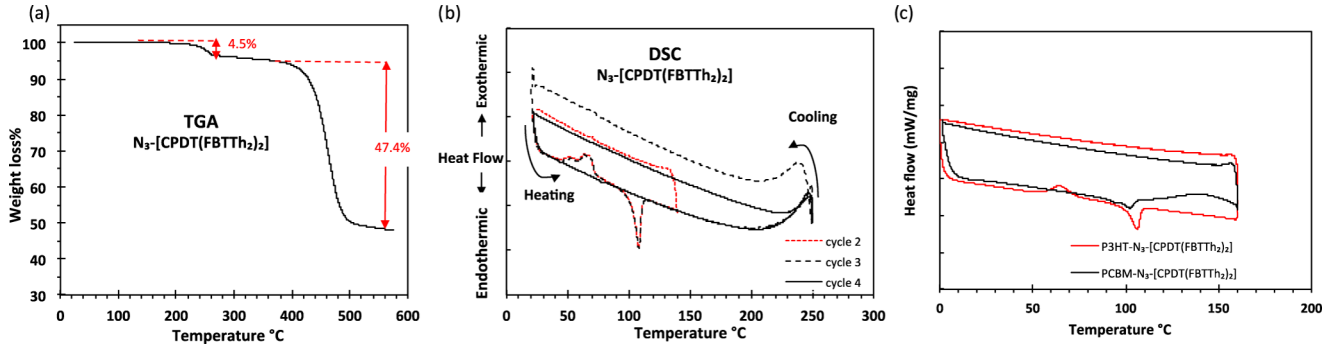

Figure 2. (a) TGA of N_3-[CPDT(FBTTh$_2$)$_2$] realized at 10 °C min^{-1} under nitrogen. (b) DSC analysis of N_3-[CPDT(FBTTh$_2$)$_2$] upon thermal cycling between 0−160 °C (dotted red line, second cycle) and 25−250 °C (black line, third and fourth cycles). (c) DSC of blends P3HT:PCBM (1:1 wt) and N_3-[CPDT(FBTTh$_2$)$_2$]:$PC_{61}BM$ (0.4:1 wt).

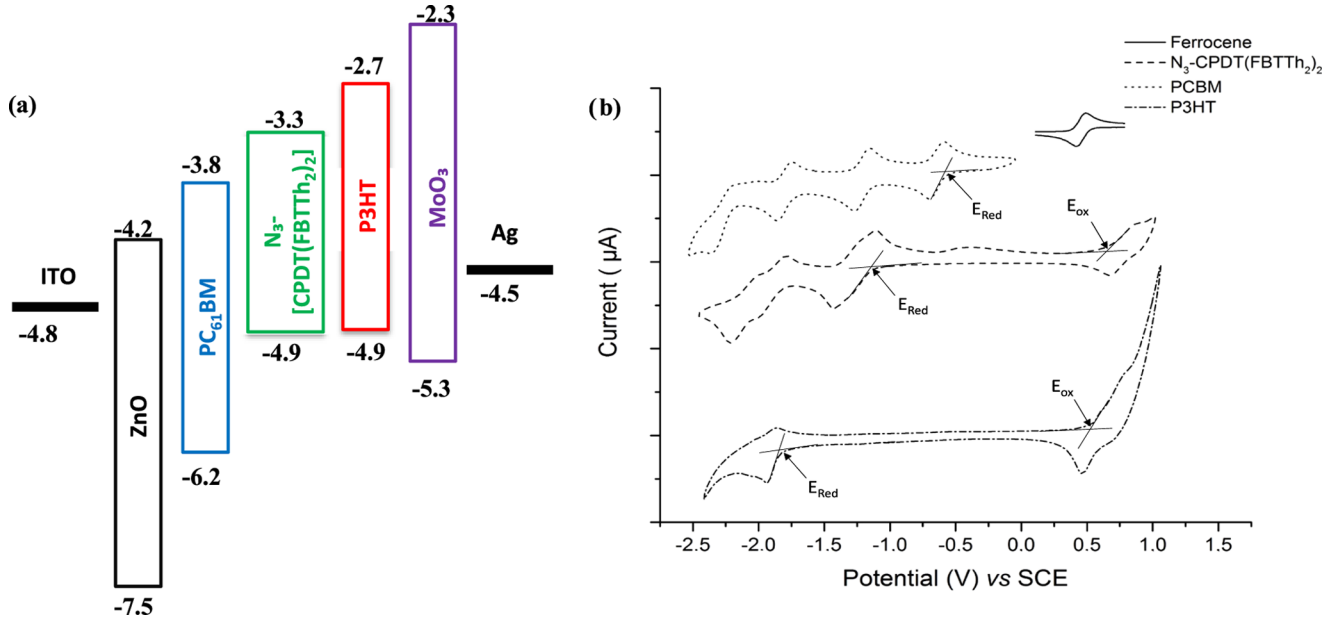

Figure 3. (a) Energy diagram of materials, (b) CV plots of 10^{-3} M P3HT, N_3-[CPDT(FBTTh$_2$)$_2$] (**6**), and $PC_{61}BM$ obtained in a CH_2Cl_2 solution containing 0.1 mol L^{-1} Bu_4NPF_6 at a scan rate of 100 mV s^{-1}. The ferrocenium/ferrocene (Fc^+/Fc) redox couple was used as an external reference ($E_{Fc^+/Fc}$ = 0.45 V/saturated calomel electrode (SCE)). Potentials are given vs those of SCE.

characteristic dinitrogen loss detected at 1341.5 g mol^{-1} definitively confirmed the presence of the azide moiety.

Second, infrared (IR) spectroscopy probes the alteration of end functionalization of [CPDT (FBTTh$_2$)$_2$] (Figure S10). After removal of the TBDMS protecting group, a broad absorption feature associated with OH-band stretching (ν_{OH} = 3500−3700 cm^{-1}) could be identified. The formation of the azide functionality was visualized from the complete disappearance of the OH group and appearance of an asymmetric characteristic vibration of azide (ν_{N_3} = 2090 cm^{-1}). The characteristic IR stretching vibration of azide at 2090 cm^{-1} was reduced to 8% of the original signal after thermal treatment at 150 °C for 10 min in the presence of PCBM, indicating an almost complete reaction of the azide group (Figure S12).

Thermogravimetric analysis (TGA) and differential scanning calorimetry (DSC) were used to probe the stability and thermal properties of N_3-[CPDT(FBTTh$_2$)$_2$], respectively (Figure 2). According to TGA, a weight loss of 4.5% between 200 and 350 °C revealed elimination of four nitrogen atoms (theoretically representing 4% of the total M_w). DSC was performed in several cycles below 160 °C and near 250 °C to determine the melting and crystallization temperatures and identify the formation of nitrene, respectively. Below 160 °C, the molecule exhibited a melting transition at 108 °C and a cold crystallization within three transitions between 40 and 73 °C (second cycle). This behavior was fully reversible and highly stable up to 160 °C. Upon heating to 250 °C (third cycle), an exothermic signal revealed the decomposition of the azide group at 180 °C, in agreement with TGA, and the formation of highly reactive nitrene by its triplet sensitization,[37] which could react with the neighboring molecules, leading to the formation of cross-links and disrupting the organization. The corresponding DSC cycle was irreversible, as no transition was observed for the fourth cycle. We also carried out DSC experiments on N_3-[CPDT(FBTTh$_2$)$_2$] mixed with P3HT or $PC_{61}BM$, to specify the activation temperature needed for the cross-linking reaction and prove its selectivity. The DSC curves of the additive before and after adding P3HT remained similar, which confirmed the selectivity of the reaction between the molecule and $PC_{61}BM$, where an exothermic peak at about 120 °C was visualized (Figure 2c). We noticed that the thermal stability of molecule **6** (160 < T > 180 °C) was higher than the

DOI: 10.1021/acsomega.6b00476
ACS Omega 2017, 2, 1340−1349

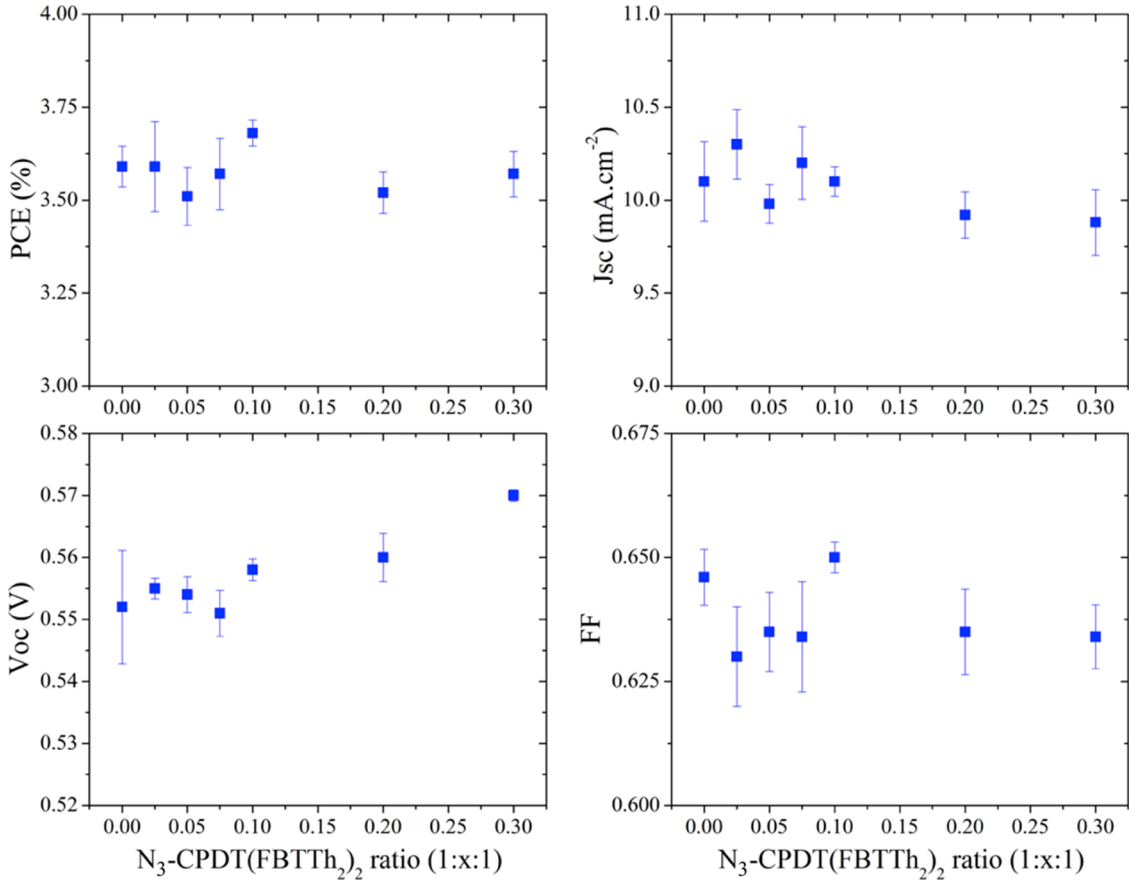

Figure 4. Evolution of PCE, J_{sc}, V_{oc}, and FF for devices with ternary blends of different ratios (P3HT:N_3-[CPDT($FBTTh_2$)$_2$]:$PC_{61}BM$), after the cross-linking reaction; values are extracted from $J(V)$ curves.

Table 1. J_{sc} Extracted from $J(V)$ Curves and from EQE spectra. Reference corresponds to the Ratio: 1:0:1

		J_{sc} from EQE (mA cm^{-2})		
ratios	J_{sc} from J(V) curves (mA cm^{-2})	between 300 and 800 nm	between 300 and 650 nm/difference with the reference	between 650 and 800 nm/differencewith the reference
1:0:1	10.22	10.25	10.00	0.25
1:0.025:1	10.48	10.29	9.98/−0.02	0.32/+0.07
1:0.05:1	10.06	10.16	9.77/−0.13	0.39/+0.14
1:0.075:1	10.26	10.13	9.72/−0.18	0.41/+0.16
1:0.1:1	10.16	10.12	9.65/−0.35	0.47/+0.22
1:0.2:1	9.93	9.83	9.17/−0.83	0.66/+0.41
1:0.3:1	9.94	9.65	8.86/−1.14	0.79/+0.54

temperature needed (110−140 °C)[38] to covalently link N_3-[CPDT($FBTTh_2$)$_2$] to $PC_{61}BM$ at the two six-membered rings via 1,3-dipolar cycloaddition,[39] forming a stable BHJ AL morphology.

Energy-level matching between AL materials is also a requirement for optimum device functionality. The highest occupied molecular orbital (HOMO) and lowest unoccupied molecular orbital (LUMO) energy levels of P3HT, N_3-[CPDT($FBTTh_2$)$_2$], and $PC_{61}BM$ were estimated via cyclic voltammetry (CV) from the onset of the oxidation and reduction potentials of the redox curves (Figure 3). Assuming that the energy levels were not affected when the materials were in the blend, the electrochemical band gap of N_3-[CPDT-($FBTTh_2$)$_2$] was calculated to be 1.6 eV. This molecule behaves as an acceptor, on the basis of the positions of its HOMO and LUMO levels with respect to those of P3HT. The exciton generated in P3HT could be transferred to N_3-[CPDT-($FBTTh_2$)$_2$], and the excitons generated by N_3-[CPDT-($FBTTh_2$)$_2$] could be dissociated into charge carriers at the interface with $PC_{61}BM$. The electrons transport to the cathode through channels formed by $PC_{61}BM$, and the holes at N_3-[CPDT($FBTTh_2$)$_2$] could transport to the anode directly or through channels of P3HT. This is a favorable structure, which should allow efficient charge separation and transport.[40]

Inverted organic solar cells with binary and ternary blends were fabricated as described in the Experimental Section. All devices with N_3-[CPDT($FBTTh_2$)$_2$] were annealed at 150 °C for 10 min to complete the cross-linking reaction with $PC_{61}BM$. The average PCE, J_{sc}, FF, and V_{oc} are presented in Figure 4. The PCE of all of the devices was constant, independent of the N_3-[CPDT($FBTTh_2$)$_2$] ratio. Indeed, the fill factor (FF) was slightly decreased in comparison to that of the binary blend but was independent of the ternary blend ratio. On the contrary, V_{oc} increased progressively with an increase in the N_3-

DOI: 10.1021/acsomega.6b00476
ACS Omega 2017, 2, 1340−1349

[CPDT(FBTTh$_2$)$_2$] concentration. This was an argument toward either a parallelly linked tandem cell mechanism, with independent donor networks, or the so-called alloy mechanism,[42] where two different molecules were closely intermixed and acted as an alloy with new energy levels. In our case, the cross-linked N$_3$-[CPDT(FBTTh$_2$)$_2$] and PC$_{61}$BM could act in this manner with a higher LUMO, leading to an actual increase in V_{oc}. Unexpectedly, J_{sc} showed a very small decrease with increased ratios of N$_3$-CPDT(FBTTh$_2$)$_2$. The J_{sc} values were confirmed by EQE measurements, presented in Table 1; the difference stayed in the acceptable margin of 3%. Overall, the decrease in J_{sc} was compensated by the increase in V_{oc}, which finally gave a nearly constant PCE.

To investigate the J_{sc} drop, the absorption spectra of thin film N$_3$-[CPDT(FBTTh$_2$)$_2$] and the binary and ternary blends were measured. They are presented in Figure 5a. With three

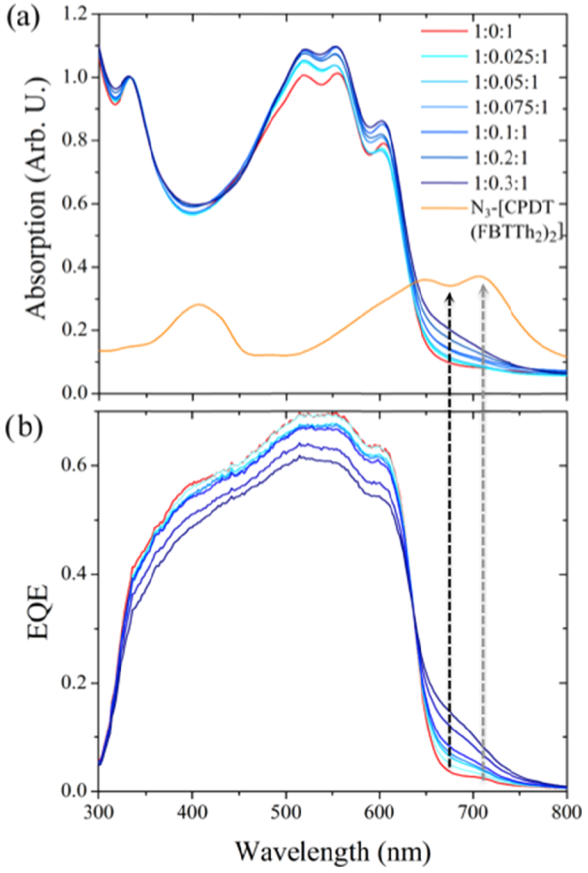

Figure 5. Evolution of (a) thin film ultraviolet−visible (UV−vis) absorption and (b) EQE for different ratios of N$_3$-[CPDT(FBTTh$_2$)$_2$], after the cross-linking step (150 °C, 10 min).

absorption bands centered at 405, 650, and 705 nm, the absorption of the additives matched perfectly the gap in the absorption of P3HT:PC$_{61}$BM. The ternary blend is expected to have a broader absorption, so more charge carriers could be generated. Indeed, the absorption band corresponding to the third component appeared from ratios as low as 1:0.05:1 and further increased with the amount of additive. However one could note that N$_3$-[CPDT(FBTTh$_2$)$_2$], being a small molecule, had a very small absorption in comparison to that of the semicrystalline polymer. A higher ratio of at least 1:0.20:1 was then necessary to exhibit a significant input from the additive. Besides, the drop before the PC$_{61}$BM band at 315 nm was reduced with the concentration of additive. This is typical of the presence of multiadduct fullerenes[41] in the AL as a marker of increased presence of cross-linked PC$_{61}$BM and an efficient cross-linking reaction between the additive and PC$_{61}$BM. The contribution of the additive in the photocurrent was confirmed on the EQE spectra presented in Figure 5b, where J_{sc} increased in the area of absorption of the bis-azide molecule (between 650 and 800 nm). However, this new contribution was counterbalanced by a progressive decrease in the contribution by P3HT and PC$_{61}$BM (between 300 and 650 nm). The equivalent current density was calculated for each domain and the difference with the reference of the binary blend was added as well. The results are summarized in Table 1. Up to a ratio of 1:0.075:1, the decrease in the P3HT:PC$_{61}$BM area was fully compensated by the contribution of the dye. For higher concentrations, the decrease was larger than the increase, leading to a limited overall J_{sc} reduction. Surprisingly, between 300 and 650 nm, the decrease in the EQE contribution of the P3HT was at the opposite of the increase of its absorption on the UV−vis spectrum. The limited thickness increase of 18 nm (9%) between the binary blend (ratio of 1:1, film thickness of 198 nm) and optimal ternary blend (ratio of 1:0.2:1, film thickness of 216 nm) (Figure S13) could not explain the J_{sc} decrease.[43,44] It could be attributed to an increase in recombination due to a less favorable morphology induced by the addition of the third component or by its cross-linking with PC$_{61}$BM.

This observation was supported by the UV−vis absorption and EQE spectra recorded on bulk heterojunctions as a function of the additive concentration (Figure 5). As already mentioned, in the solid state (Figure 5a, brown spectrum), the small molecule showed two characteristic vibronics at 650 nm (black dashed arrow) and 705 nm (gray dashed arrow), attesting its crystalline domains. However, in the ternary blends, the 705 nm absorption band was absent, signifying that the small molecule should be homogeneously dispersed in the bulk or that it formed amorphous domains. In a same manner, the crystallization of P3HT remained effective, but to a lesser extent (Figure 5a and Table S1, ratio between optical densities at 555 and 605 nm extracted from Figure 5), with the addition of the cross-linker. Indeed, the absorption spectra of P3HT:PCBM showed the absorption band of PCBM (340 nm) and that of P3HT (450−650 nm), with three well-known vibronic transitions of P3HT. The first two transitions (at 525 and 555 nm) were attributed to the $\pi-\pi^*$ transition, and the shoulder at 605 nm was due to interchain interactions. Upon incorporation of the bis-azide molecule in the P3HT:PCBM blend, an increase in the absorption strength of P3HT along with a slight modification of the relative intensities of the vibronic peaks ($OD_{605\ nm}/OD_{555\ nm}$) was observed. The decrease in the $OD_{605\ nm}/OD_{555\ nm}$ ratio upon addition of an additive (0−0.05) was directly related to a decrease in the intermolecular coupling and a lower crystallization of P3HT. For higher concentrations of the additive (0.075−0.3), the decrease in $OD_{605\ nm}$ was compensated by an increase in the absorption band of the additive itself at 650 nm. As a result, the $OD_{605\ nm}/OD_{555\ nm}$ ratio increased. Even if a slight decrease in the $OD_{605\ nm}/OD_{555\ nm}$ ratio was observed, the sharp vibronic peak located at 605 nm attested the crystallinity of P3HT. As a consequence, most of the small molecules were certainly ejected from the crystalline domains of P3HT to the interface with PCBM. As a result, the reaction with PCBM was almost complete.

DOI: 10.1021/acsomega.6b00476
ACS Omega 2017, 2, 1340−1349

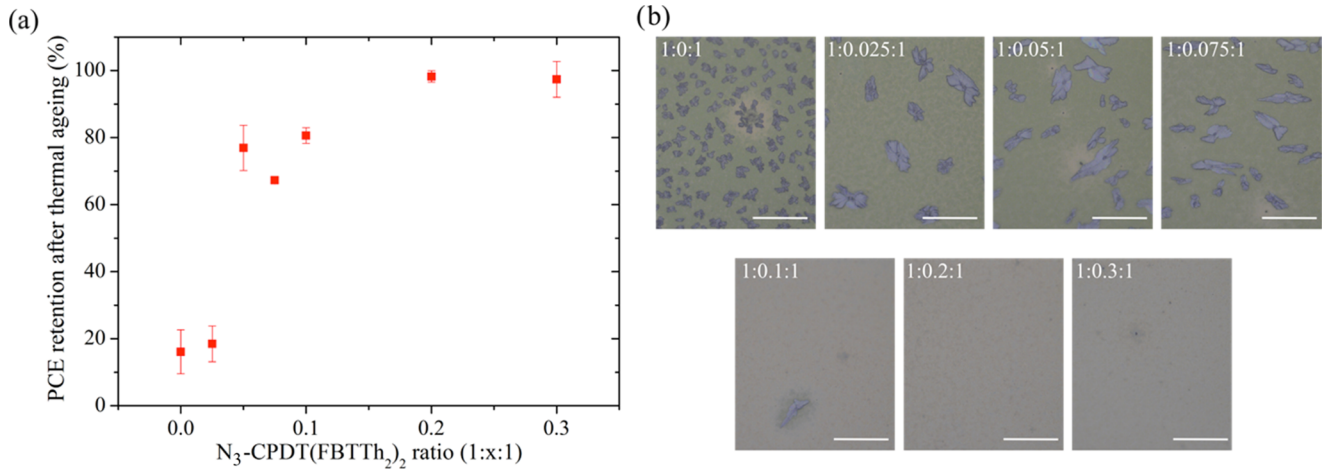

Figure 6. (a) Evolution of the PCE retention in percentage after thermal ageing at 150 °C for 24 h. (b) Microscope images of the corresponding AL, scale bar is 50 μm.

To summarize, despite the fact that the J_{sc} did not increase with an increase in the concentration of N_3-[CPDT-$(FBTTh_2)_2$], PCE stayed constant irrespective of concentration. This is not always the case in terms of the additive for thermal stabilization, where we could see a decrease in PCE with the an increase in additive concentration after the cross-linking reaction, as, for example, with the DAZH.[26] This effect is directly due to the contribution by the additive in J_{sc} and the V_{oc} increase.

Finally, thermal stabilization was investigated. After deposition of the AL, the samples were exposed to accelerated thermal ageing at 150 °C for 24 h; then, the top electrode was deposited and the devices were characterized. PCE retention in comparison to that in pristine devices is presented in Figure 6a. The devices made with the binary blend showed a poor retention of less than 20%. This was the result of phase segregation between the donor and acceptor and the apparition of $PC_{61}BM$ aggregates, visible in the microscope images of the AL presented in Figure 6b. With the increase in the amount of bis-azide CPDT$(FBTTh_2)_2$, the PCE after ageing was less and less affected, until it reached full stabilization at a ratio of 1:0.2:1. At this concentration, no $PC_{61}BM$ clusters were observed on the microscope images anymore. This retention of 100% of the initial efficiency even after aggressive thermal ageing at 150 °C for 24 h was better than that of other reported additives, such as BABP (92% after 24 h at 150 °C) or DAZH (82% after 130 h at 85 °C).[24,38] Furthermore at such a concentration, the equivalent number of $PC_{61}BM$ molecules per azide was 3.8, whereas for our previously described cross-linker, BABP,[24] at the optimized concentration, this ratio was of 2.9. Less of the new additive was necessary to thermally stabilize the blend.

CONCLUSIONS

In conclusion, the synthesis of a bis-azide cross-linker with a wide absorption (up to 800 nm) and high molar mass (1386.8 g mol^{-1}) was demonstrated for the first time to elaborate a stable morphology at elevated temperature. This new molecule has a modular (D^1-A–D^2-A–D^1) architecture and bears an azide functional group on both undecyl alkane chains of the central CPDT unit. The high purity and good thermal stability of the molecule were evaluated by TGA and HPLC characterization. Effective and complete cross-linking of the azide group with $PC_{61}BM$ at the two six-membered rings occurred between 130 and 150 °C according to DSC and IR measurements. The frontier orbital energy levels of the molecule measured by CV were well suited with the P3HT-PCBM system for efficient charge separation and transportation. This molecule combined a double functionality for the blend: it broadened the absorption of the AL, contributed to the global current of the cells, and acted as a thermal stabilizer. In comparison to other existing additives, this one showed 100% stabilization because the PCE was maintained at its original value after curing of the azide and thermal ageing. So far, this cross-linker is the most performing additive to retain PCE during thermal ageing.

MATERIALS

All reactions involving air-sensitive reagents were carried out under a dried nitrogen atmosphere, using dried glassware, unless otherwise stated. CPDT was purchased from TCI. All other chemicals and solvents were purchased from Aldrich (France) and ABCR (Germany). These chemicals were used as received, without any further purification. Anhydrous THF was obtained using a solvent purification system (SPS-800). 5′-Hexyl-2,2′-bithiophene-5-trimethylstannane (D^1), 4,7-dibromo-5-fluorobenzo[*c*][1,2,5]thiadiazole (A), and 4-bromo-5-fluoro-7-(5′-hexyl-[2,2′-bithiophene]-5-yl)benzo[*c*][1,2,5]thiadiazole (D^1-A) were prepared by methods similar to those reported in the literature.[29−31]

Synthesis of (11-Bromoundecanyloxy)(*tert*-butyl)-dimethylsilane (1). 11-Bromo-1-undecanol (10 g, 0.040 mmol) was dissolved in (200 mL) THF in the presence of air. Imidazole (3 g, 0.044 mmol) and *tert*-butylchlorodimethylsilane (6.6 g, 0.044 mmol) were added simultaneously into the mother solution, and precipitation was observed. The solution was stirred at 60 °C overnight. The mixture was poured into 200 mL of water and extracted with 100 mL of hexane. The organic layer was washed with water and dried over anhydrous magnesium sulfate (Mg_2SO_4). After concentrating the solution, the crude product was purified by silica gel column chromatography using a mixture of hexane and ethyl acetate (75:25 v/v) as the eluent, followed by evaporation of the solvent, yielding a colorless liquid (yield = 85%).

^{1}H NMR (400 MHz, $CDCl_3$): (ppm) 3.56 (t, 2H), 3.36 (t, 2H), 1.82 (m, 2H), 1.54−1.232 (m, 16H), 0.847 (s, 9H), 0.01 (s, 6H).

DOI: 10.1021/acsomega.6b00476
ACS Omega 2017, 2, 1340−1349

Synthesis of 4-4′-Bis(((*tert*-butyl)dimethylsilyloxy)-undecyl)dicyclopenta[2,1-*b*:3,4-*b*′]dithiophene (2). Ground potassium hydroxide (KOH, 500 mg, 9 mmol) and potassium iodide (25 mg) were added to a suspension of 4*H*-cyclopenta[2,1-*b*:3,4-*b*′]dithiophene (400 mg, 2.243 mmol) in DMSO (20 mL). The mixture was then degassed three times and filled with nitrogen gas. After stirring for 30 min, (11-bromoundecanyloxy)(*tert*-butyl)dimethylsilane (**1**) (2 g, 5 mmol) was added dropwise. A change in the color to green was observed after the addition of the first drop. The reaction was quenched with water after agitating for 24 h at room temperature (r.t.). The product was extracted with hexane and washed with aq. NH_4Cl. The crude product was purified by silica gel column chromatography using pentane/DCM (100:0 to 80:20) (v/v) as the eluent. The desired product was obtained as a light yellow oil (yield = 85%).

^{1}H NMR (400 MHz, $CDCl_3$): (ppm) 7.1 (d, 2H), 6.68 (d, 2H), 3.54 (t, 2H), 1.8 (m, 4H), 1.5−1 (m, 36H), 0.9−0.8 (m, 18H), 0.01 (s, 12H).

Synthesis of 2,6-Di-(trimethyltin)-4-4′-bis(((*tert*-butyl)-dimethylsilyloxy)undecyl)dicyclopenta[2,1-*b*:3,4-*b*′]-dithiophene (3). *n*-Butyl lithium solution (BuLi) in hexane (2.5 M, 0.65 mL, 1.6 mmol) was added dropwise to a stirred solution of 4-4′-bis(((*tert*-butyl)dimethylsilyloxy)undecyl)-dicyclopenta[2,1-*b*:3,4-*b*′]dithiophene (**2**) (300 mg, 0.4 mmol) in dry THF (4 mL) at −78 °C. After complete addition, the liquid-nitrogen bath was removed immediately to increase the temperature to r.t. and the mixture was further stirred for 1 h. After cooling to −78 °C, trimethyltin chloride (Me_3SnCl, 1 M, 2 mL, 2 mmol) was added slowly. Finally, the solution was suddenly warmed by replacing the liquid-nitrogen bath with a water bath and stirring for 18 h before pouring into deionized (DI) water. Extraction was performed using diethylether and by repeated washing with DI water. Drying over anhydrous Mg_2SO_4, filtering, and solvent evaporation gave a crude product, which was placed under high vacuum for 24 h (to remove excess trimethyltin chloride) to yield a yellow viscous oil (yield ∼98%), which was used in the next step without further purification.

^{1}H NMR (400 MHz, $CDCl_3$): (ppm) 6.89 (d, 2H), 3.54 (t, 2H), 1.8 (m, 4H), 1.5−1 (m, 36H), 0.9−0.8 (m, 18H), 0.03 (s, 18H), 0.01 (s, 12H).

Synthesis of 4-4′-Bis(((*tert*-butyl)dimethylsilyloxy)-undecyl)dicyclopenta[2,1-*b*:3,4-*b*′]dithiophene-bis(5-fluoro-7-(5′-hexyl-[2,2′-bithiophene]-5-yl)benzo[*c*]-[1,2,5]thiadiazole) (4). To a 10 mL microwave vial equipped with a sealed septum were added 2,6-di-(trimethyltin)-4-4′-bis(((*tert*-butyl)dimethylsilyloxy)undecyl)dicyclopenta[2,1-*b*:3,4-*b*′]dithiophene (**3**) (210 mg, 0.196 mmol), 4-bromo-5-fluoro-7-(5′-hexyl-[2,2′-bithiophene]-5-yl)benzo[*c*][1,2,5]-thiadiazole (190 mg, 0.4 mmol), $Pd(PPh_3)_4$ (20 mg, 8.5%), and anhydrous chlorobenzene (2 mL). The vial was heated in a microwave reactor at 100 °C (5 min), 110 °C (5 min), 120 °C (5 min), 140 °C (5 min), and 160 °C (120 min). Upon cooling, the resulting viscous blue liquid was concentrated. The crude product was placed in a Soxhlet thimble and washed with copious amounts of methanol and ethanol. Then, the product was purified by silica gel column chromatography twice using as the eluent a mixture of pentane and chloroform (100:0 to 50:50) (v/v). The product was recovered as a metallic sticky purple solid (yield = 65%).

^{1}H NMR (400 MHz, $CDCl_3$): (ppm) 8.20 (s, 2H), 8.01(d, 2H), 7.70 (d, 2H), 7.174 (d, 2H), 7.109 (d, 2H), 6.719 (d, 2H), 3.52 (t, 4H), 2.805 (t, 4H), 2.02 (m, 4H), 1.72 (m, 4H), 1.5−1.05 (m, 48H), 0.913−0.88 (m, 24H), 0.01 (s, 12H). ^{13}C APT NMR (100 MHz, $CDCl_3$): (ppm) 159.42, 157.20, 153.21, 149.78, 146.42, 140.38, 136.04, 134.42, 134.26, 128.97, 125.06, 124.32, 124.05, 123.84, 115.92, 63.33, 54.13, 37.90, 32.88, 31.60, 31.57, 30.27, 30.11, 29.63, 29.58, 29.44, 28.80, 26.48, 25.99, 25.79, 24.71, 22.60, 18.37, 14.11, −5.25. MALDI-TOFMS *m*/*z* calculated for $C_{83}H_{112}F_2N_4O_2S_8Si_2$ = 1546.61 g mol^{-1}; found = 1546.6 g mol^{-1}. HPLC showed a purity of 99% using a gradient of cyclohexane/DCM (90−98). UV−vis absorbance ($CHCl_3$) λ_{max} = 601 nm, λ_{onset} = 690 nm. UV−vis absorbance (spin-coated film from $CHCl_3$ solution) λ_{max} = 646, 711 nm, λ_{onset} = 785 nm. TGA shows that degradation of the molecule occurs through two steps, with weight loss % of 5.89 and 59.5% over temperature ranges of 210−374 and 374−540 °C, respectively. DSC reveals that **4** exhibits a melting transition at 114 °C, a crystallization transition at 43 °C, and cold crystallization at 69 °C after the first cycle.

Synthesis of 4-4′-Bis(1-undecanol)dicyclopenta[2,1-*b*:3,4-*b*′]dithiophene-bis(5-fluoro-7-(5′-hexyl-[2,2′-bithiophene]-5-yl)benzo[*c*][1,2,5]thiadiazole) (5). The TBDMS-protected derivative (**4**) (170 mg, 0.1 mmol) was dissolved in 20 mL of THF containing HCl (0.2 g, 2 mmol). The mixture was allowed to react for 30 min at r.t. After full conversion (checked by thin-layer chromatography), the mixture was neutralized with trimethylamine, concentrated, precipitated in methanol, filtered, and purified by silica gel column chromatography using pentane/chloroform (90:10 to 0:100) (v/v) as the eluent. The product was recovered as a metallic purple solid (yield = 95%).

^{1}H NMR (400 MHz, $CDCl_3$): (ppm) 8.20 (s, 2H), 8.01(d, 2H), 7.70 (d, 2H), 7.174 (d, 2H), 7.109 (d, 2H), 6.719 (d, 2H), 3.55 (t, 4H), 2.805 (t, 4H), 2.02 (m, 4H), 1.72 (m, 4H), 1.5−1.05 (m, 48H), 0.91 (t, 6H). ^{13}C APT NMR (100 MHz, $CDCl_3$): (ppm) 159.40, 153.07, 149.70, 146.40, 140.51, 140.36, 136.01, 134.41, 128.95, 125.04, 124.49, 124.26, 124.04, 123.82, 116.17, 63.08, 54.11, 37.83, 32.79, 31.60, 31.56, 30.27, 30.05, 29.57, 29.54, 29.40, 29.37, 28.81, 25.71, 24.68, 22.61, 14.11. (Disappearance of peaks [26.46 (CH_3), 18.37(C), −5.25 (CH_3)] related to the OTBDMS function). MALDI-TOFMS *m*/*z* calculated for $C_{71}H_{84}F_2N_4O_2S_8$ = 1318.34 g mol^{-1}; found = 1318.4 g mol^{-1}. UV−vis absorbance ($CHCl_3$) λ_{max} = 607 nm, λ_{onset} = 685 nm. UV−vis absorbance (spin-coated film from $CHCl_3$ solution) λ_{max} = 630, 720 nm, λ_{onset} = 800 nm. TGA shows that the degradation of the molecule occurs through a single step, starting at 326 °C and ending at 540 °C. The residual mass of the material at 580 °C is 35.6% of the initial mass. DSC reveals that **5** exhibits a melting transition at 140 °C and a crystallization temperature of 88 °C.

Synthesis of 4-4′-Bis(1-azido)undecane)dicyclopenta-[2,1-*b*:3,4-*b*′]dithiophene-bis(5-fluoro-7-(5′-hexyl-[2,2′-bithiophene]-5-yl)benzo[*c*][1,2,5]thiadiazole) (6). Triphenylphosphine PPh_3 (170 mg, 0.6 mmol) and bis-alcohol-functionalized CPDT(FBTTh$_2$)$_2$ (**5**) (100 mg, 0.072 mmol) were dissolved in anhydrous THF (10 mL). The solution was stirred at 0 °C, purged with nitrogen bubbling, and shielded from light. Then, DIAD (120 mg, 0.6 mmol) and $(PhO)_2P(O)N_3$ (166 mg, 0.6 mmol) were added successively. After 3 h, the mixture was concentrated and the product was precipitated in methanol. The crude product was purified by another precipitation in methanol to obtain the desired product as a metallic purple solid (yield = 90%).

DOI: 10.1021/acsomega.6b00476
ACS Omega 2017, 2, 1340−1349

^{1}H NMR (400 MHz, $CDCl_3$): (ppm) 8.20 (s, 2H), 8.01(d, 2H), 7.70 (d, 2H), 7.174 (d, 2H), 7.109 (d, 2H), 6.719 (d, 2H), 3.17 (t, 4H), 2.805 (t, 4H), 2.02 (m, 4H), 1.72 (m, 4H), 1.5−1.05 (m, 48H), 0.91 (t, 6H). ^{13}C APT NMR: (100 MHz, $CDCl_3$): (ppm) 159.36, 153.16, 149.72, 146.40, 140.51, 140.36, 136.01, 134.41, 128.95, 125.04, 124.49, 124.26, 124.04, 123.82, 116.17, 54.11, 51.47, 37.85, 31.61, 31.57, 30.28, 30.07, 29.56, 29.49, 29.45, 29.38, 29.13, 28.82, 25.87, 24.69, 22.61, 14.11. The peak at 63.3 ppm (CH_2−OH) disappeared and a new peak at 51.47 ppm (CH_2N_3) appeared. MALDI-TOFMS m/z calculated for $C_{71}H_{84}F_2N_{10}S_8$ = 1368.45 g mol^{-1}; found = 1368.5 g mol^{-1}.

EXPERIMENTAL SECTION

Device Fabrication. All of the devices have the same structure: glass/indium tin oxide (ITO)/ZnO/AL/MoO_3/Ag. ITO-coated glass was cleaned in successive solutions of soap dissolved in deionized water, pure deionized water, and isopropanol for 15 min under ultrasonication. After drying the substrate in air, UV−ozone treatment (10 min) was applied to the substrate to increase the hydrophilic nature of the surface and remove residual organic contamination. The ZnO precursor was prepared by dissolving zinc acetate dihydrate (Sigma-Aldrich) in 0.15 mol L^{-1} absolute ethanol and adding 0.15 mol L^{-1} monoethanolamine (Sigma-Aldrich). The solution was stirred for 2 h at 50 °C and then spin-coated on the cleaned ITO substrates at 2000 rpm for 60 s. The films were then annealed at 180 °C over 1 h. The final ZnO thickness was 40 nm. All further elaboration and characterization steps were carried out in an inert atmosphere in gloveboxes. Solutions of P3HT and $PC_{61}BM$ (20 mg mL^{-1}) were prepared with a weight ratio of 1:1, heated at 85 °C for 15 min, and then kept at 50 °C overnight. A mother solution of fresh N_3-[CPDT(FBTTh$_2$)$_2$] was prepared (0.5−6 mg mL^{-1}) and added to the binary solutions directly before spin-coating. The ternary solutions were stirred at r.t. for 30 min in a tinted vial. The AL was spun at 1000 rpm over 40 s. To obtain an optimized morphology, the samples were then immediately transferred into glass Petri dishes, in which they could slowly dry.[32] After solvent annealing, the substrates were annealed at 150 °C for 10 min to complete the cross-linking reaction between N_3-[CPDT(FBTTh$_2$)$_2$] and $PC_{61}BM$. Finally, the MoO_3 (7 nm) and Ag (70 nm) top electrodes were thermally evaporated. For each condition, two substrates containing four cells of 10 mm^2 were fabricated. In this way series data contain up to eight values. This allows us to calculate the average and standard deviations of PCE, the FF, the short-circuit density current (J_{sc}), and the open-circuit voltage (V_{oc}). Current density versus voltage, $J(V)$, curves were obtained for each devices using Keithley 2400, under an AM1.5 sun-simulator with a Xenon lamp, calibrated with a radiometer (IM1400) at 100 mW cm^{-2}. The samples were eventually encapsulated by gluing a glass substrate on top of the electrode with NOA61 glue (Epotecny). EQE was estimated outside the glovebox with a setup consisting of a Xenon lamp connected to a Horiba monochromator coupled with a picoamperemeter. Besides the full devices, ALs were deposited directly on quartz substrates. Absorption spectra were recorded using a UV−vis spectrophotometer (Safas Monaco MC2). Optical imaging was performed with a magnification 50× (Zeiss microscope). The AL thickness was measured with a profilometer (α step IQ).

ASSOCIATED CONTENT

Supporting Information

The Supporting Information is available free of charge on the ACS Publications website at DOI: 10.1021/acsomega.6b00476.

Experimental procedures and Figures S1−S13 (PDF)

AUTHOR INFORMATION

Corresponding Authors

*E-mail: guillaume.wantz@ims-bordeaux.fr (G.W.).
*E-mail: olivier.dautel@enscm.fr (O.J.D.).

ORCID

Olivier J. Dautel: 0000-0003-2327-5376

Author Contributions

§H.A. and T.G. contributed equally.

Author Contributions

The manuscript was written through contributions from all authors. All authors have given approval to the final version of the manuscript.

Notes

The authors declare no competing financial interest.

ACKNOWLEDGMENTS

The authors are grateful to the Agence Nationale de la Recherche (ANR) for funding the ANR-HABISOL-2010-003 (PROGELEC) program "CEPHORCAS" and the ANR-PROGELEC-2013 program "HELIOS".

REFERENCES

(1) Zhao, J.; Li, Y.; Yang, G.; Jiang, K.; Lin, H.; Ade, H.; Ma, W.; Yan, H. Efficient organic solar cells processed from hydrocarbon solvents. *Nat. Energy* **2016**, *1*, No. 15027.

(2) Kaltenbrunner, M.; White, M. S.; Głowacki, E. D.; Sekitani, T.; Someya, T.; Sariciftci, N. S.; Bauer, S. Ultrathin and lightweight organic solar cells with high flexibility. *Nat. Commun.* **2012**, *3*, No. 770.

(3) Machui, F.; Hosel, M.; Li, N.; Spyropoulos, G. D.; Ameri, T.; Sondergaard, R. R.; Jorgensen, M.; Scheel, A.; Gaiser, D.; Kreul, K.; Lenssen, D.; Legros, M.; Lemaitre, N.; Vilkman, M.; Valimaki, M.; Nordman, S.; Brabec, C. J.; Krebs, F. C. Cost analysis of roll-to-roll fabricated ITO free single and tandem organic solar modules based on data from manufacture. *Energy Environ. Sci.* **2014**, *7*, 2792−2802.

(4) Zhang, Q.; Kan, B.; Liu, F.; Long, G.; Wan, X.; Chen, X.; Zuo, Y.; Ni, W.; Zhang, H.; Li, M.; Hu, Z.; Huang, F.; Cao, Y.; Liang, Z.; Zhang, M.; Russell, T. P.; Chen, Y. Small-molecule solar cells with efficiency over 9%. *Nat. Photonics* **2014**, *9*, 35−41.

(5) Coughlin, J. E.; Henson, Z. B.; Welch, G. C.; Bazan, G. C. Design and Synthesis of Molecular Donors for Solution-Processed High-Efficiency Organic Solar Cells. *Acc. Chem. Res.* **2014**, *47*, 257−270.

(6) Min, J.; Jiao, X.; Sgobba, V.; Kan, B.; Heumüller, T.; Rechberger, S.; Spiecker, E.; Guldi, D. M.; Wan, X.; Chen, Y.; Ade, H.; Brabec, C. J. High efficiency and stability small molecule solar cells developed by bulk microstructure fine-tuning. *Nano Energy* **2016**, *28*, 241−249.

(7) Shaheen, S. E.; Brabec, C. J.; Sariciftci, N. S.; Padinger, F.; Fromherz, T.; Hummelen, J. C. 2.5% efficient organic plastic solar cells. *Appl. Phys. Lett.* **2001**, *78*, 841−843.

(8) Peet, J.; Kim, J. Y.; Coates, N. E.; Ma, W. L.; Moses, D.; Heeger, A. J.; Bazan, G. C. Efficiency enhancement in low-bandgap polymer solar cells by processing with alkane dithiols. *Nat. Mater.* **2007**, *6*, 497−500.

(9) Li, G.; Shrotriya, V.; Yao, Y.; Yang, Y. Investigation of annealing effects and film thickness dependence of polymer solar cells based on poly(3-hexylthiophene). *J. Appl. Phys.* **2005**, *98*, No. 043704.

(10) Dang, M. T.; Hirsch, L.; Wantz, G. P3HT:PCBM, Best Seller in Polymer Photovoltaic Research. *Adv. Mater.* **2011**, *23*, 3597−3602.

DOI: 10.1021/acsomega.6b00476
ACS Omega 2017, 2, 1340−1349

(11) Halls, J. J. M.; Pichler, K.; Friend, R. H.; Moratti, S. C.; Holmes, A. B. Exciton diffusion and dissociation in a poly(p-phenylenevinylene)/C60 heterojunction photovoltaic cell. *Appl. Phys. Lett.* **1996**, *68*, 3120−3122.
(12) Campoy-Quiles, M.; Ferenczi, T.; Agostinelli, T.; Etchegoin, P. G.; Kim, Y.; Anthopoulos, T. D.; Stavrinou, P. N.; Bradley, D. D. C.; Nelson, J. Morphology evolution via self-organization and lateral and vertical diffusion in polymer:fullerene solar cell blends. *Nat. Mater.* **2008**, *7*, 158−164.
(13) Yang, X.; van Duren, J. K. J.; Janssen, R. A. J.; Michels, M. A. J.; Loos, J. Morphology and Thermal Stability of the Active Layer in Poly(p-phenylenevinylene)/Methanofullerene Plastic Photovoltaic Devices. *Macromolecules* **2004**, *37*, 2151−2158.
(14) Nam, C.-Y.; Qin, Y.; Park, Y. S.; Hlaing, H.; Lu, X.; Ocko, B. M.; Black, C. T.; Grubbs, R. B. Photo-Cross-Linkable Azide-Functionalized Polythiophene for Thermally Stable Bulk Heterojunction Solar Cells. *Macromolecules* **2012**, *45*, 2338−2347.
(15) Mueller, C. J.; Klein, T.; Gann, E.; McNeill, C. R.; Thelakkat, M. Azido-Functionalized Thiophene as a Versatile Building Block To Cross-Link Low-Bandgap Polymers. *Macromolecules* **2016**, *49*, 3749−3760.
(16) Kim, B. J.; Miyamoto, Y.; Ma, B.; Fréchet, J. M. J. Photocrosslinkable Polythiophenes for Efficient, Thermally Stable, Organic Photovoltaics. *Adv. Funct. Mater.* **2009**, *19*, 2273−2281.
(17) Waters, H.; Kettle, J.; Chang, S.-W.; Su, C.-J.; Wu, W.-R.; Jeng, U. S.; Tsai, Y.-C.; Horie, M. Organic photovoltaics based on a crosslinkable PCPDTBT analogue; synthesis, morphological studies, solar cell performance and enhanced lifetime. *J. Mater. Chem. A* **2013**, *1*, 7370−7378.
(18) Griffini, G.; Douglas, J. D.; Piliego, C.; Holcombe, T. W.; Turri, S.; Fréchet, J. M. J.; Mynar, J. L. Long-Term Thermal Stability of High-Efficiency Polymer Solar Cells Based on Photocrosslinkable Donor-Acceptor Conjugated Polymers. *Adv. Mater.* **2011**, *23*, 1660−1664.
(19) Cheng, Y.-J.; Hsieh, C.-H.; Li, P.-J.; Hsu, C.-S. Morphological Stabilization by In Situ Polymerization of Fullerene Derivatives Leading to Efficient, Thermally Stable Organic Photovoltaics. *Adv. Funct. Mater.* **2011**, *21*, 1723−1732.
(20) Wojciechowski, K.; Ramirez, I.; Gorisse, T.; Dautel, O.; Dasari, R.; Sakai, N.; Hardigree, J. M.; Song, S.; Marder, S.; Riede, M.; Wantz, G.; Snaith, H. J. Cross-Linkable Fullerene Derivatives for Solution-Processed n−i−p Perovskite Solar Cells. *ACS Energy Lett.* **2016**, 648−653.
(21) Diacon, A.; Derue, L.; Lecourtier, C.; Dautel, O.; Wantz, G.; Hudhomme, P. Cross-linkable azido C60-fullerene derivatives for efficient thermal stabilization of polymer bulk-heterojunction solar cells. *J. Mater. Chem. C* **2014**, *2*, 7163−7167.
(22) Chen, C.-P.; Huang, C.-Y.; Chuang, S.-C. Highly Thermal Stable and Efficient Organic Photovoltaic Cells with Crosslinked Networks Appending Open-Cage Fullerenes as Additives. *Adv. Funct. Mater.* **2015**, *25*, 207−213.
(23) Png, R.-Q.; Chia, P.-J.; Tang, J.-C.; Liu, B.; Sivaramakrishnan, S.; Zhou, M.; Khong, S.-H.; Chan, H. S. O.; Burroughes, J. H.; Chua, L.-L.; Friend, R. H.; Ho, P. K. H. High-performance polymer semiconducting heterostructure devices by nitrene-mediated photocrosslinking of alkyl side chains. *Nat. Mater.* **2010**, *9*, 152−158.
(24) Derue, L.; Dautel, O.; Tournebize, A.; Drees, M.; Pan, H.; Berthumeyrie, S.; Pavageau, B.; Cloutet, E.; Chambon, S.; Hirsch, L.; Rivaton, A.; Hudhomme, P.; Facchetti, A.; Wantz, G. Thermal Stabilisation of Polymer−Fullerene Bulk Heterojunction Morphology for Efficient Photovoltaic Solar Cells. *Adv. Mater.* **2014**, *26*, 5831−5838.
(25) Derue, L.; Lecourtier, C.; Gorisse, T.; Hirsch, L.; Dautel, O.; Wantz, G. A solvent additive to enhance the efficiency and the thermal stability of polymer:fullerene solar cells. *RSC Adv.* **2015**, *5*, 3840−3843.
(26) Rumer, J. W.; Ashraf, R. S.; Eisenmenger, N. D.; Huang, Z.; Meager, I.; Nielsen, C. B.; Schroeder, B. C.; Chabinyc, M. L.; McCulloch, I. Dual Function Additives: A Small Molecule Crosslinker for Enhanced Efficiency and Stability in Organic Solar Cells. *Adv. Energy Mater.* **2015**, *5*, No. 1401426.
(27) Chao, Y.-C.; Chuang, C.-H.; Hsu, H.-L.; Wang, H.-J.; Hsu, Y.-C.; Chen, C.-P.; Jeng, R.-J. Enhanced thermal stability of organic photovoltaics via incorporating triphenylamine derivatives as additives. *Sol. Energy Mater. Sol. Cells* **2016**, *157*, 666−675.
(28) Verstappen, P.; Cardinaletti, I.; Vangerven, T.; Vanormelingen, W.; Verstraeten, F.; Lutsen, L.; Vanderzande, D.; Manca, J.; Maes, W. Impact of structure and homo-coupling of the central donor unit of small molecule organic semiconductors on solar cell performance. *RSC Adv.* **2016**, *6*, 32298−32307.
(29) van der Poll, T. S.; Love, J. A.; Nguyen, T.-Q.; Bazan, G. C. Non-Basic High-Performance Molecules for Solution-Processed Organic Solar Cells. *Adv. Mater.* **2012**, *24*, 3646−3649.
(30) kang, S.; Kang, M. S.; Park, J. W.; Kang, P.; Yi, M. H.; Kwon, S.-K.; Kim, Y.-H. Synthesis and studies on 2-hexylbithiophene end-capped oligomer for OTFT. *Curr. Appl. Phys.* **2010**, *10*, e166−e170.
(31) Medlej, H.; Nourdine, A.; Awada, H.; Abbas, M.; Dagron-Lartigau, C.; Wantz, G.; Flandin, L. Fluorinated benzothiadiazole-based low band gap copolymers to enhance open-circuit voltage and efficiency of polymer solar cells. *Eur. Polym. J.* **2014**, *59*, 25−35.
(32) Chambon, S.; Derue, L.; Lahaye, M.; Pavageau, B.; Hirsch, L.; Wantz, G. MoO3 Thickness, Thermal Annealing and Solvent Annealing Effects on Inverted and Direct Polymer Photovoltaic Solar Cells. *Materials* **2012**, *5*, 2521.
(33) Raju, T. B.; Gopikrishna, P.; Iyer, P. K. Highly efficient and facile alkylation of 4 H-cyclopenta-[2,1-b:3,4-b[prime or minute]]-dithiophene in water. *RSC Adv.* **2014**, *4*, 37738−37745.
(34) Murray, K. A.; Holmes, A. B.; Moratti, S. C.; Rumbles, G. Conformational changes in regioregular polythiophenes due to crosslinking. *J. Mater. Chem.* **1999**, *9*, 2109−2116.
(35) Murray, K. A.; Holmes, A. B.; Moratti, S. C.; Friend, R. H. The synthesis and crosslinking of substituted regioregular polythiophenes. *Synth. Met.* **1996**, *76*, 161−163.
(36) Kesters, J.; Verstappen, P.; Raymakers, J.; Vanormelingen, W.; Drijkoningen, J.; D'Haen, J.; Manca, J.; Lutsen, L.; Vanderzande, D.; Maes, W. Enhanced Organic Solar Cell Stability by Polymer (PCPDTBT) Side Chain Functionalization. *Chem. Mater.* **2015**, *27*, 1332−1341.
(37) Scriven, E. F. V.; Turnbull, K. Azides: their preparation and synthetic uses. *Chem. Rev.* **1988**, *88*, 297−368.
(38) Kim, H. J.; Han, A. R.; Cho, C.-H.; Kang, H.; Cho, H.-H.; Lee, M. Y.; Fréchet, J. M. J.; Oh, J. H.; Kim, B. J. Solvent-Resistant Organic Transistors and Thermally Stable Organic Photovoltaics Based on Cross-linkable Conjugated Polymers. *Chem. Mater.* **2012**, *24*, 215−221.
(39) Bräse, S.; Gil, C.; Knepper, K.; Zimmermann, V. Organic Azides: An Exploding Diversity of a Unique Class of Compounds. *Angew. Chem., Int. Ed.* **2005**, *44*, 5188−5240.
(40) Ameri, T.; Khoram, P.; Min, J.; Brabec, C. J. Organic Ternary Solar Cells: A Review. *Adv. Mater.* **2013**, *25*, 4245−4266.
(41) Distler, A.; Sauermann, T.; Egelhaaf, H.-J.; Rodman, S.; Waller, D.; Cheon, K.-S.; Lee, M.; Guldi, D. M. The Effect of PCBM Dimerization on the Performance of Bulk Heterojunction Solar Cells. *Adv. Energy Mater.* **2014**, *4*, No. 1300693.
(42) Lu, L.; Kelly, M. A.; You, W.; Yu, L. Status and prospects for ternary organic photovoltaics. *Nat. Photonics* **2015**, *9*, 491−500.
(43) Lenes, M.; Koster, L. J. A.; Mihailetchi, V. D.; Blom, P. W. M. Thickness dependence of the efficiency of polymer:fullerene bulk heterojunction solar cells. *Appl. Phys. Lett.* **2006**, *88*, No. 243502.
(44) Morvillo, P.; Bobeico, E.; Esposito, S.; Diana, R. Effect of the Active Layer Thickness on the Device Performance of Polymer Solar Cells Having [60]PCBM and [70]PCBM as Electron Acceptor. *Energy Procedia* **2012**, *31*, 69−73.

DOI: 10.1021/acsomega.6b00476
ACS Omega 2017, 2, 1340−1349